Microchemical Journal 219 (2025) 116140

Contents lists available at ScienceDirect

Microchemical Journal

journal homepage: www.elsevier.com/locate/microc

Label-free electrochemical DNA biosensor for detection of peanut allergen Ara h2 based on gold nanoparticles-modified self-assembled monolayers in food matrices

Juan Pablo Hervás-Pérez, Marta Sánchez-Paniagua *

Department of Chemistry in Pharmaceutical Sciences, Faculty of Pharmacy, Complutense University of Madrid, 28040 Madrid, Spain

ARTICLE INFO

Keywords:
Peanut allergen
Self assembled monolayer
Gold nanoparticles
DNA biosensor
Electrochemical

ABSTRACT

A label-free electrochemical genosensor for the detection of Ara h2, a major peanut allergen, has been developed using mixed self-assembled monolayers (SAMs) for DNA immobilization. The study used a sandwich format and compared gold nanoparticles-modified screen printed carbon electrodes (AuNPs-SPCE) and screen printed gold electrodes to obtain a highly sensitive bioplatform. Different binary and ternary SAMs were evaluated as sensing phase, by electrochemical impedance spectroscopy and cyclic voltammetry, obtained the best signal to noise ratio with CP-DTT-AuNPs-SPCE. The genosensor demonstrated a linear response in the concentration range of 0.025–10 nM, with a detection limit of 0.02 nM by square wave voltammetry. The precision of the biosensor was validated, showing a RSD of less than 8 % across different concentrations. Selectivity tests confirmed negligible signals for non-complementary sequences. Additionally, the method proved effective in real food matrices, with recovery rates between 95.0 % and 105.5 % in spiked soy-based beverage and low-fat cow's milk.

1. Introduction

Access to sufficient, safe and nutritious food is fundamental for sustaining life and promoting good health. Food safety therefore remains a priority for public health authorities, particularly in light of emerging risks such as food allergies. These disorders, defined as adverse immune responses to specific food proteins, are increasingly recognized as a global health issue due to their growing prevalence and potentially life-threatening consequences [1,2]. Within the European Union, Regulation (EU) No 1169/2011 requires the labelling of fourteen major allergens, including eggs, fish, milk, soybeans and peanuts, to ensure consumer protection [3].

Peanuts (*Arachis hypogaea L.*) are widely consumed as a nutritious legume crop and are increasingly incorporated into functional foods owing to their protein, lipid and micronutrient content. However, they are also among the most potent allergenic foods. Even trace amounts of peanut proteins can elicit severe reactions in sensitized individuals, ranging from mild cutaneous symptoms to anaphylaxis, a potentially fatal condition requiring immediate medical intervention [4–6].

To date, at least eight major allergenic proteins (Ara h1–Ara h8) have been characterized in peanuts. Among them, Ara h1, Ara h2 and Ara h3 are considered the most clinically relevant, with Ara h2 consistently identified as the most potent and the best predictor of severe allergic reactions, particularly in children [7–9]. IgE reactivity to Ara h2 is strongly associated with systemic responses, and recent studies demonstrate that monoclonal antibodies against this protein can prevent peanut-induced anaphylaxis in murine models [10].

Given these risks, the development of analytical methods for peanut allergen detection in food matrices is of great importance for both industry and consumers. Current methodologies fall into two main categories: protein-based immunoassays and DNA-based molecular approaches. Enzyme-linked immunosorbent assays (ELISA), mass spectrometry and polymerase chain reaction (PCR) are the most widely implemented techniques, offering high sensitivity and specificity [11,12]. However, they also present limitations, such as high cost, time-consuming protocols and the need for specialized equipment, which restrict their use in routine food control.

In recent years, electrochemical biosensors have emerged as promising alternatives, offering advantages such as miniaturization, cost-effectiveness, rapid response and potential for on-site analysis [13–18]. Most reported devices for peanut allergen detection are immunosensors or aptasensors. For instance, a dual electrochemical immunosensor was developed for the simultaneous detection of Ara h 1 and Ara h 6 in food matrices, achieving low detection limits and good

* Corresponding author.
E-mail addresses: jphervas@ucm.es (J.P. Hervás-Pérez), martasan@ucm.es (M. Sánchez-Paniagua).

https://doi.org/10.1016/j.microc.2025.116140
Received 7 October 2025; Received in revised form 1 November 2025; Accepted 9 November 2025
Available online 10 November 2025

performance in processed samples [19]. A microfluidic origami nanoaptasensor was also reported for Ara h 1, enabling sensitive detection in just 20 min [20]. More recently, nanobody-based electrochemical immunoassays have been proposed as robust alternatives to conventional antibodies, offering improved stability and sensitivity [21].

Nevertheless, commercial food processing, particularly through thermal or high-pressure treatments, can alter protein conformation and immunoreactivity, compromising the reliability of protein-based assays [22]. This challenge has encouraged the development of DNA-based detection strategies, which target specific nucleotide sequences encoding allergenic proteins and are unaffected by protein denaturation. Electrochemical genosensors, in particular, represent an attractive option due to their high selectivity, low cost and compatibility with automation [23]. Despite the great analytical properties of these devices, their application to the detection of DNA sequences encoding peanut allergens is very limited. Different studies have demonstrated the feasibility of DNA biosensors for peanut allergens. For example, Sun et al. developed a stem-loop probe-based DNA sensor for Ara h1 with successful application in food matrices [24]. The same authors, proposed two different strategies to enhance Ara h1 DNA biosensor performance, involving a multilayer graphene–gold nanocomposite [25] and chitosan–multiwalled carbon nanotube [26] that provides high conductivity, large surface area, and strong signal amplification. Also, a voltammetric inmunosensor was developed to detect the peanut allergen Ara h6 in foodstuff using a sandwich-type format with gold nanoparticle-modified electrodes and electrochemical silver detection [27]. More recently, novel biosensing strategies have been introduced, such as disposable amperometric tools for peanut detection by targeting a chloroplast DNA marker in processed foods [28].

To our knowledge, only two studies reported the development of DNA biosensing platforms for Ara h2 detection. In 2014, Sánchez-Paniagua et al. described a selective electrochemical genosensor for this peanut allergen, employing a sandwich format on gold electrodes with optimized self-assembled monolayers and fine-tuning through a Design of Experiments approach [29]. In 2017, a SAM based on ternary monolayers were prepared using anti-fluorescein peroxidase for electrochemical Ara h2 detection [30]. Despite progress in protein-based biosensors, reports of genosensors specifically targeting Ara h2 remain scarce, especially in label-free formats. Given the clinical relevance of this allergen and the advantages of unlabeled electrochemical biosensors—such as speed, cost-effectiveness, and minimal reagent use—we present a DNA-based label free electrochemical biosensor for Ara h2 detection as a contribution to peanut allergen monitoring in food safety.

2. Experimental

2.1. Procedures

2.1.1. Electrode surface modification protocol

The immobilization protocol of the capture probe onto the working electrode was based on the strong affinity interaction between thiol groups and gold (SH–Au). For this purpose, the capture probe was functionalized with a thiol moiety, which enables its stable attachment to gold surfaces. Two different immobilization strategies were employed: i) direct deposition of thiolated CP onto SPEAu and ii) CP immobilzed onto SCPE modified with gold nanoparticles (AuNPs-SPCE). The latter approach was expected to provide a larger surface area and numerous active binding sites, thereby enhancing the subsequent immobilization of the capture probe [31–34]. In both cases, the sensing interface was completed by the formation of a self-assembled monolayer (SAM) on the electrode surface, consisting of the use of a blocking agent, which served to minimize nonspecific adsorption and ensure optimal probe accessibility. Fig. 1 provides a schematic overview of the label-free biosensor preparation.

First, screen-printed gold and carbon electrodes were washed with water and ethanol and dried with nitrogen. After, the SPEAu electrodes were conditioned to improve the sensitivity and reproducibility by an electrochemical pretreatment of 25 cyclic voltammetric scans in a 0.5 M H_2SO_4 solution, between 0 and 1.6 V at 100 mVs^{-1}, until a stable cyclic voltammogram was obtained.

A volume of 15 μL of the CP solution was carefully deposited onto the clean gold working electrode surface and incubated at 4 °C for a defined period of time. Following, the electrode was thoroughly rinsed with 2xSPEE buffer to remove weakly adsorbed or non-specifically bound DNA molecules (Fig. 1A and B). In AuNPs-SPCE, 10 μL of the nanoparticles suspension was first dispensed onto the electrode surface and allowed to dry completely, thereby generating a nanostructured gold layer. The immobilization steps described above were then applied to these modified electrodes. At this stage, however, the direct immobilization of thiolated single-stranded DNA of CP typically results in the formation of a disordered monolayer due to non-specific adsorption of

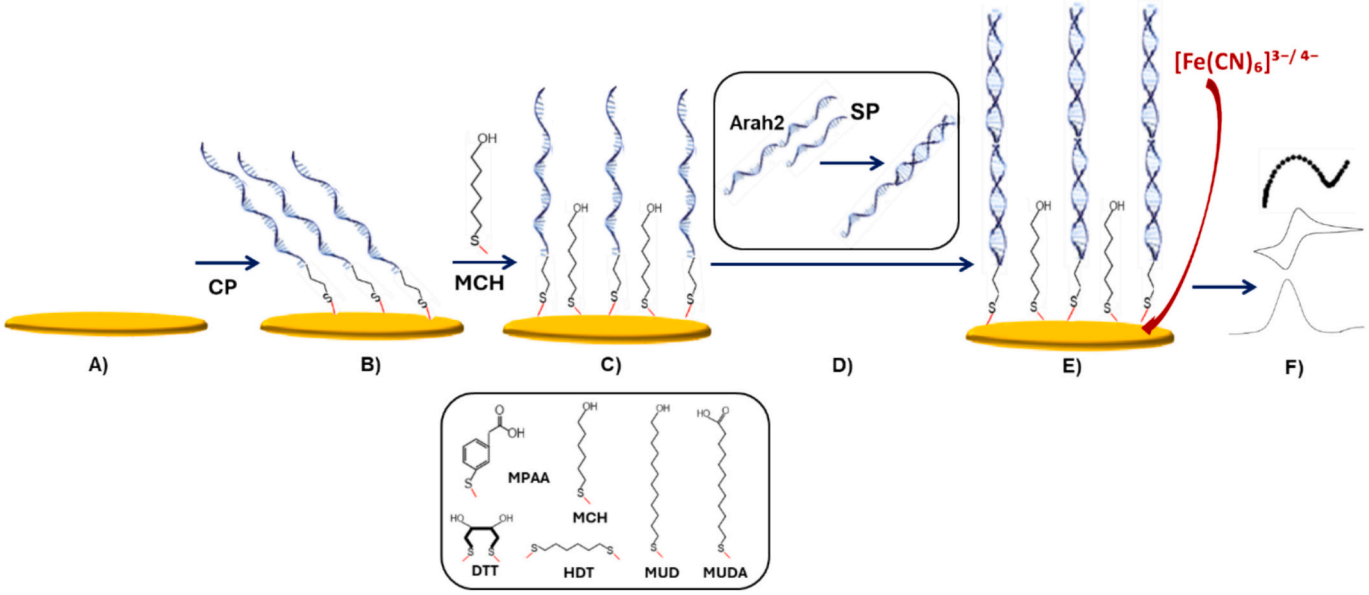

Fig. 1. Scheme of the label-free biosensor preparation procedure.

the probes onto the electrode surface.

To achieve more controlled and homogeneous surface coverage, a binary SAM was generated with an alkanethiol spacer. 15 μL of diluent solution was added to the electrode surface and incubated for a defined time, enabling the displacement of non-specifically bound probes and the orderly arrangement of CP strands (Fig. 1C). Finally, the electrodes were rinsed with 2 × SSPE buffer to remove excess blocking and unbound molecules, resulting in a stable and well-oriented sensing interface. Ternary SAM with a two-step immobilization process was also employed. In this case, 15 μL of the thiolated capture probe (CP) solution mixed with the selected diluent (HDT, DTT, MPAA, MUD, or MUDA) at variable concentrations were deposited onto the working electrode and incubated overnight in a humidified chamber. After incubation, the electrode was rinsed with 2 × SSPE buffer and dried under a gentle nitrogen stream. Subsequently, 15 μL of 0.5 mM MCH were added and incubated for 30 min to form the ternary monolayer interfaces. Finally, the sensors were rinsed with Milli-Q water and dried under nitrogen.

The hybridization assay was carried out in a sandwich format, which involved two sequential steps: an initial homogeneous hybridization in solution, followed by a heterogeneous hybridization on the electrode surface. In the first step, the homogeneous hybridization reaction between the signaling probe and the target DNA was performed in 2xSPEE buffer(Fig. 1D). To ensure efficient denaturation and subsequent renaturation, the solution was heated to 95 °C for 5 min, rapidly cooled in an ice-water bath for 5 min, and then incubated at 25 °C for a defined period of time to promote hybrid formation. Immediately after this step, 15 μL of the hybridization mixture was applied onto the modified electrode and incubated at room temperature, allowing the target-probe complex to specifically hybridize with the capture probe (Fig. 1E). After heterogeneous hybridization, the working electrode was carefully rinsed with 2xSPEE buffer to remove non-specifically adsorbed DNA sequences, ensuring a selective recognition event at the sensing interface.

Importantly, performing the assay in a sandwich-type format—-where the capture probe attached to the electroe anchors the target, and a signaling probe binds to a different region of the same sequence—-provides an additional level of specificity and produce signal amplification that significantly enhances the electrochemical response [35,36]. This dual recognition strategy not only reduces background signals arising from non-specific adsorption but also amplifies the detectable signal through the subsequent binding of reporter molecules.

Electrochemical detection was performed using a label-free approach, in which the ferri/ferrocyanide redox couple served as an external probe (Fig. 1F). Upon hybridization with the target, a complete DNA duplex was formed on the electrode surface, thereby creating a physical and electrostatic barrier to electron transfer. The consequent modulation of the redox signal provided an indirect yet reliable measure of DNA recognition events.

2.2. Electrochemical measurements

Electrochemical impedance spectroscopy (EIS) and cyclic voltammetry (CV) were employed to study the interface properties of the modified electrode surface during the fabrication procedure of the genosensor. Square wave voltammetry (SWV) was used for quantitative analysis.

CV experiments were performed in 5 mM $[Fe(CN)_6]^{3-/4-}$ prepared in 0.1 M KCl, within a potential window of −0.10 to +0.60 V at a scan rate of 50 mV s^{-1}. EIS measurements were conducted using the same redox probe, starting at the open circuit potential (OCP) with a sinusoidal perturbation of 5 mV (peak-to-peak) over a frequency range from 10^6 to 0.1 Hz. The resulting spectra were fitted to a Randles equivalent circuit to extract the values of the circuit component, including charge transfer resistance (R_{ct}), solution resistance (RΩ), the constant phase element (CPE) associated with double-layer capacitance, and Warburg impedance (Zw). The Nyquist plots exhibited a high-frequency semicircle, characteristic of electron-transfer kinetics, followed by a low-frequency linear region indicative of diffusion-controlled processes. The semicircle diameter provided a direct measure of R_{ct}. The increased R_{ct} values were consistent with successful assembly of different compounds onto the sensor surface. SWV was conducted at a scan rate of 25 mV s^{-1}, with a modulation amplitude of 50 mV and frequency of 25 Hz. The current response in 5 mM $[Fe(CN)_6]^{3-/4-}$ (0.1 M KCl) was monitored, and variations in the cathodic peak current were quantitatively correlated with the target analyte concentration.

3. Results and discussion

3.1. Electrochemical characterization of biosensor fabrication steps

The interfacial properties of the electrode surface during fabrication were investigated by EIS using $[Fe(CN)_6]^{3-/4-}$ as the redox probe, a technique highly sensitive to biorecognition events at the surface–electrolyte interface. An additional study using hexamine ruthenium $(Ru(NH_3)_6^{3+/2+})$ as a redox probe was attempted; however, a well-defined semicircle in the Nyquist plot was not observed in the experiences, likely due to electrostatic interactions between the positively charged Ru complex at pH 7.4 and the negatively charged DNA layer. Overall, $[Fe(CN)_6]^{3-/4-}$ proved to be the most suitable redox probe for both EIS-based optimization.

A bare screen-printed carbon electrode (SPCE) exhibited a charge transfer resistance (R_{ct} of 752 Ω) as shown by the semicircle in the Nyquist plot (Fig. 2A, black curve). As expected, modification of the electrode surface with gold nanoparticles (AuNPs-SPCE) resulted in a decrease in R_{ct} to 485 Ω (yellow curve), indicating enhanced accessibility of the redox probe due to the higher conductivity and large surface area of the modified electrode.

The immobilization of the capture probe onto the gold-modified surface (CP-AuNPs-SCPE) occurred through the stable anchoring of the biomolecule to the electrode via covalent S—Au bond formation, requiring the prior assembly of a self-assembled monolayer (SAM) with a blocking agent. This step ensured the vertical orientation of the capture probe, favoring efficient hybridization with the target sequence. As observed in the Nyquist plot, SAM formation (MCH-CP-AuNPs-SCPE) in the electrode surface increased R_{ct} to 1425 Ω, confirming the successful immobilization of the DNA strand. Subsequent addition of the Ara h2–SP hybrid led to a further increase in R_{ct} to 1874 Ω, verifying the specific binding of the analyte to the capture probe and the formation of the complete duplex.

To investigate the specificity of the CP-Ara h2 hybridization, two control experiments were carried out (inset Fig. 2A). In the first, the electrochemical response of a bio-platform prepared without capture probe (SP-Ara h2-MCH-AuNPs-SCPE, control a, grey line) was compared with that of MCH-AuNPs-SCPE alone (red line). Both platforms displayed very similar charge transfer resistance values (R_{ct} 875 Ω vs. 780 Ω), confirming that the binding of the analyte (Ara h2 probe) occurs exclusively in the presence of the immobilized capture probe on the electrode surface. A second control experiment was performed using a biosensor constructed in the absence of analyte, SP-MCH-CP-AuNPs-SCPE (control b, purple line). In this case, the electrochemical response was comparable to MCH-CP-AuNPs-SCPE platform (green line) with R_{ct} values of 1430 and R_{ct} 1370 Ω, respectively, supporting that SP not binding in the electrode surface in absence of Ara h2. These results demonstrate that specific Ara h2 recognition takes place only when CP, SP and analyte are present and the small differences observed in the control measurements can be attributed to minor non-specific adsorption events at the electrode surface. Such non-specific effects, although limited, will be further addressed in the following sections.

Cyclic voltammetry (CV) measurements were also conducted to validate the EIS results (Fig. 2B). The bare SPCE displayed a typical reversible redox process with a peak current of 85.5 μA and a ΔEp of 0.13 V. After AuNPs modification, the electrode exhibited an enhanced electrochemical response due to increased conductivity, with a peak

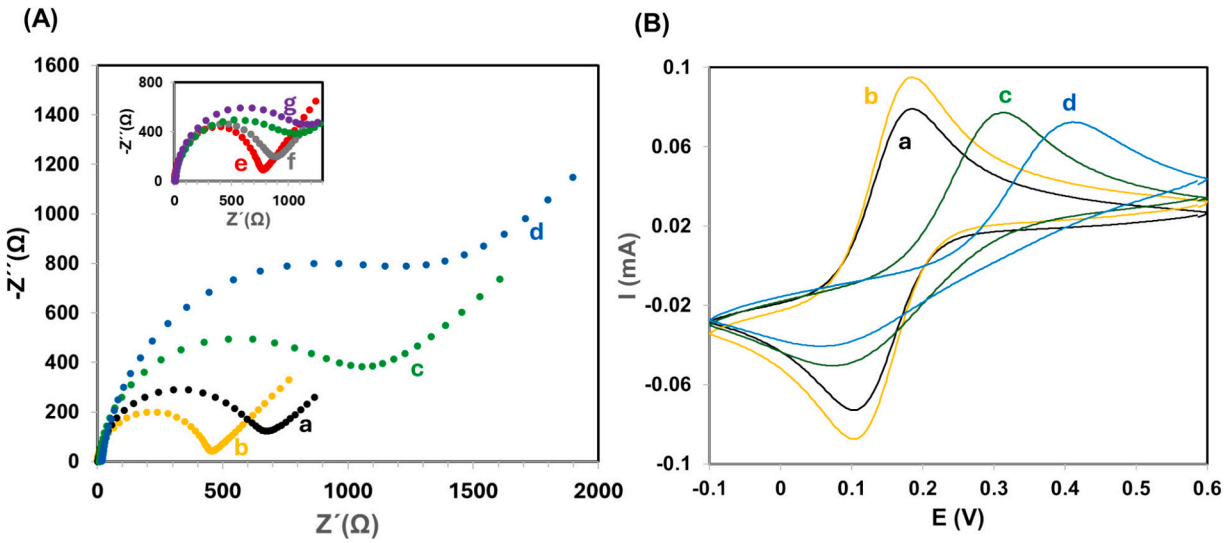

Fig. 2. Nyquist plots (A) and cyclic voltammograms (B) of 5 mM $[Fe(CN)_6]^{3-/4-}$ in 0.1 M KCl. SPCE (a, black line), AuNPs-SPCE (b, yellow line), MCH-CP-AuNPs-SPCE (c, green line) and SP-Ara h 2-MCH-CP-AuNPs-SCPE (d, blue line). Inlet: MCH-AuNPs-SCPE (e, red line), SP-Ara h 2-MCH-AuNPs-SCPE (f, grey line), SP-MCH-CP-AuNPs-SCPE (g, purple line). (For interpretation of the references to colour in this figure legend, the reader is referred to the web version of this article.)

current of 105 μA and a ΔEp of 0.09 V. These improvements indicate higher redox reversibility and more efficient electron transfer in the AuNP-SPCE, consistent with enhanced overall electrochemical activity. This result correlates with that obtained by EIS, where the R_{ct} decreased from 752 to 485 Ω upon the addition of AuNPs onto the bare SPCE. The formation of the CP–MCH self-assembled monolayer (MCH–CP–AuNPs–SPCE) on the electrode surface led to a decrease in the cyclic voltammetry parameters (Ip = 80 μA and ΔEp = 0.23 V), which correlates with the increase in R_{ct} observed in EIS measurements, confirming the successful immobilization of the CP strand. Furthermore, upon addition of the Ara h2–SP hybrid, a pronounced decrease in peak current (Ip = 50 μA) and a broader ΔEp (0.35 V) were observed, indicating the formation of a duplex structure between the three DNA probes.

A second CP immobilization strategy was evaluated using SPEAu, where thiolated DNA capture probes were directly deposited onto the electrodes, exploiting the strong thiol–gold affinity. The resulting SAM (MCH–CP–SPEAu) showed an R_{ct} of 1057 Ω, lower than that obtained with the AuNPs–modified electrodes (MCH–CP–AuNPs–SPCE, R_{ct} = 1425 Ω). The higher R_{ct} in the latter indicates more extensive CP immobilization, as increased DNA coverage hinders electron transfer, confirming that gold nanoparticle incorporation enhances probe loading by enlarging the electrode surface area and the number of active sites. Comparison of the impedimetric response to Ara h2, expressed as the signal-to-background (S/N) ratio, showed values of 1.15 for SPEAu and 1.53 for AuNPs-SCPE, indicating more sensitive response in the last case. Accordingly, AuNPs-modified SCPEs were selected as the electrochemical bio-platform for subsequent experiments.

3.2. Study of different self-assembled monolayers as sensing phase

In this study, a range of short- and long-chain thiol-based diluents, including mono- and dithiols as well as aromatic and aliphatic structures, with or without additional functional groups (hydroxyl or carboxyl), were evaluated as blocking component in SAM formation. Specifically, three short-chain thiols with 3C/6C alkane backbones were tested: two aliphatic diluents—mercaptohexanol (MCH) and 1,6-hexanedithiol (HDT)—bearing one or two thiol groups with and without hydroxyl functionalities, respectively and one aromatic diluent, mercaptophenylacetic acid (MPAA) that contain one thiol and carboxyl groups (Fig. 1). In addition, long-chain monothiols with 11C alkane chains, namely MUD and MUDA, bearing hydroxyl and carboxyl groups, respectively, were investigated. Both binary and ternary self-assembled monolayers (SAMs) were prepared. Binary SAMs consisted of the capture probe (CP) and one of the above mentioned diluents. Ternary interfaces were prepared through a two-step process: CP/diluent layers were first assembled on electrode surface, followed by other blocking agent addition. Since MCH has been reported as an efficient secondary spacer in ternary layers [10], MCH + third-component-CP monolayers were designed.

The analytical performance of the genosensor was assessed based on two key parameters: the signal arising from specific hybridization with the complementary target, and the background signal resulting from non-specific adsorption, collectively expressed as signal to noise ratio (S/N). This is calculated as the ratio of R_{ct} in the presence of the analyte to R_{ct} in its absence. Assays were conducted using 1 nM of Ara h2 to measure the specific response, while control experiments were performed under identical conditions in the absence of the target served to determine the blank signal. All experiments were carried out in triplicate to evaluate reproducibility and assess data variability. The concentration of the diluents used depends on whether a monothiol or a dithiol is employed, as previous studies have demonstrated that dithiols, due to the higher number of surface-binding thiol groups compared to monothiols, require lower concentrations for effective monolayer formation [37,38]. Specifically, a concentration of 1 mM was used for monothiols, whereas 1 μM was employed for dithiols. In all case, a concentration of 1 μM of CP was used.

In binary SAMs, dithiol compounds (HDT and DTT) yielded higher S/N ratios than their monothiol counterparts (Fig. 3A). The bridge-like configuration formed on the electrode surface, owing to the presence of two thiol groups, affords greater surface coverage and thereby minimises non-specific molecular adsorption. This is evidenced by the low background signals observed in the absence of the analyte. Furthermore, the dual anchoring points promote a spacing effect between immobilized DNA probes, which reduces steric hindrance and facilitates the hybridization process, as reflected in the higher signal intensities recorded in the presence of the target. Among the two dithiols evaluated, DTT yielded superior results (S/N of 3.86 for DTT-CP SAM vs 3.21 for HDT-CP SAM). This diluent contains two hydroxyl groups capable of forming intermolecular hydrogen bonds, potentially giving rise to a pseudo-layer that enhances hybridization efficiency by promoting a more ordered spatial arrangement of the probe layer. Short-chain

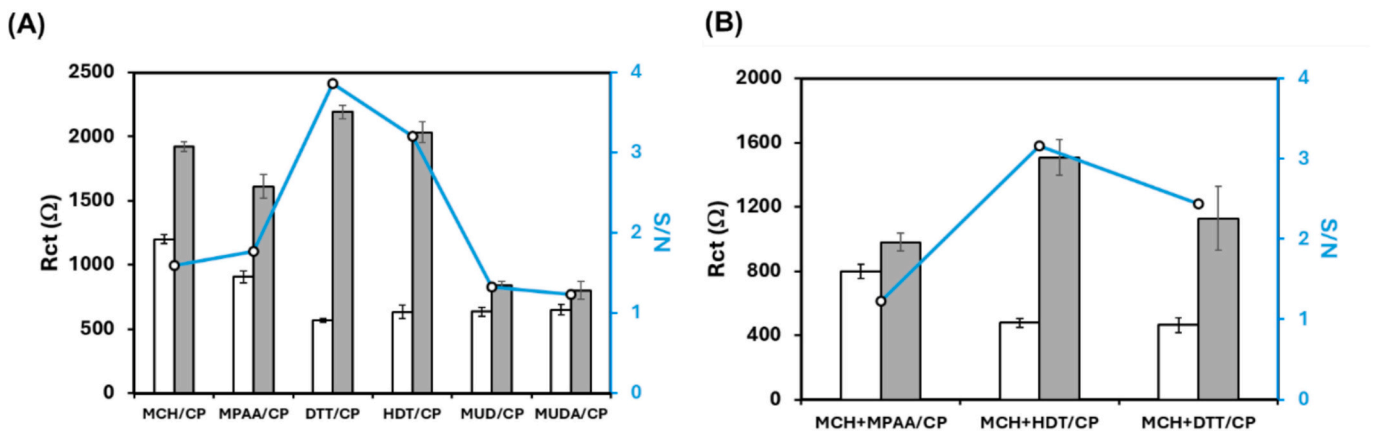

Fig. 3. Optimization of the sensing phase using binary (A) and ternary (B) SAMs. Blank signal (white bars) and analyte signal (grey bars) are shown. The resulting S/B values are represented by the blue line. Error bars represent the standard deviation ($n = 3$). Experimental conditions: 1 h CP immobilization (1 μM), 30 min incubation with diluent (1 mM for monothiols and 1 μM for dithiols), homogeneous hybridization with 1 nM Ara h2 and 1 μM SP for 15 min, followed by 1 h heterogeneous hybridization. (For interpretation of the references to colour in this figure legend, the reader is referred to the web version of this article.)

diluents containing one thiol group (MCH and MPAA) exhibited poorer S/N ratios, with reductions of approximately 2.4-fold for MCH and 2.2-fold for MPAA compared to the DTT-CP SAM (Fig. 3A). Although MPAA contains an aromatic ring that could contribute to greater rigidity and a favourable orientation for probe exposure, no improvement in analyte signal was observed with this diluent. This may be attributed to possible electrostatic repulsion between the negatively charged carboxylic groups of MPAA and the phosphate backbone of the DNA thereby reducing hybridization efficiency. In contrast, MCH, a diluent bearing a hydroxyl group, is more neutral and less electrostatically interactive, which may enhance target recognition by reducing stacking interactions and facilitating probe accessibility showing signal in presence of Ara h2 higher to MPAA-based SAMs However, this monolayer resulted in a larger background current, indicative of a greater susceptibility to nonspecific adsorption.

On the other hand, self-assembled monolayers (SAMs) prepared using two long-chain monothiol diluents — MUD (bearing a hydroxyl group) and MUDA (with a carboxyl group) were also evaluated. However, these diluents proved unsuitable for this purpose. While their longer alkyl chains (C11) promote molecular ordering and result in a more hydrophobic environment near the electrode surface, leading to a more compact monolayer that effectively suppresses nonspecific signals and reduces background current comparing C6 short-chain monothiol diluents (e.g., $R_{ct} = 635$ Ω for MUD vs $R_{ct} = 1200$ Ω for MCH), they also hinder probe accessibility. Specifically, the 11-carbon alkyl chains of these diluents exceed the length of the CP spacer, potentially allowing the diluent molecules to encounter the first bases of the immobilized capture probes. Since hybridization initiates at the 5′ end of the CP — the region closest to the electrode — this spatial obstruction is likely to reduce the accessibility of the target sequence to the probe, resulting in diminished analyte signals in MUD- or MUDA-based CP-AuNPs-SCPE platforms. Furthermore, as observed with MPAA, MUDA contains deprotonated carboxyl groups under the working pH conditions, which may introduce additional electrostatic repulsion with the negatively charged phosphate backbone of the target DNA strand, further impairing hybridization efficiency (S/N of 1.23 for MUDA/CP SAM and S/N of 1.33 for MUD).

Ternary self-assembled monolayers (SAMs) were evaluated using mercaptohexanol (MCH) as a secondary diluent alongside either hexanedithiol (HDT), dithiothreitol (DTT), or mercaptophenylacetic acid (MPAA) (Fig. 3B). The use of long-chain diluents was excluded due to their poor performance in binary SAM systems. Among the three ternary configurations, the system incorporating HDT exhibited the highest S/N ratio (3.16), indicative of enhanced hybridization efficiency and reduced non-specific adsorption. This superior performance can be attributed to the linear and flexible aliphatic structure of HDT, which, owing to its two anchoring points, promotes the formation of a more homogeneous and densely packed monolayer when co-assembled with MCH. Consequently, the background signal is reduced compared with the corresponding binary monolayers ($R_{ct} = 477$ Ω for MCH + HDT-CP vs. $R_{ct} = 634$ Ω for HDT-CP and $R_{ct} = 1200$ Ω for MCH-CP). However, a clear decrease in the analyte-derived signal was observed, resulting in a reduction in the S/N ratio compared to the HDT-CP SAM. Conversely, although DTT yielded the best response in binary SAMs, it did not translate to improved performance in MCH + DTT-CP ternary systems. The presence of hydroxyl groups in both diluents likely introduces steric hindrance and extensive hydrogen bonding, disrupting SAM organisation and consequently reducing assay sensitivity (S/N = 2.4). In the case of MCH + MPAA-CP SAMs, the analyte signal was substantially reduced, consistent with previous observations for MPAA-CP binary monolayers. This diminished response is most likely the result of unfavourable intermolecular interactions between the negatively charged carboxylate ($–COO^-$) groups of MPAA and the hydroxyl (–OH) groups of MCH that induce surface heterogeneity. Such structural irregularities may impede hybridization efficiency by restricting probe accessibility and enhancing non-specific adsorption, thereby undermining the overall analytical performance of the sensing interface (S/N = 1.23).

3.3. Optimization of the experimental variables

To develop a highly sensitive bioplatform, an optimisation study was conducted to evaluate diferent experimental variables, includinn reagent concentrations and incubation times, with the conditions employed in Fig. 3 as the starting point. The initial optimization focused on the immobilitazion of the capture probe onto the AuNPs–SCPE surface, with particular attention to the influence of incubation time, probe concentration, and ionic strength. Incubation times between 30 and 90 min were investigated, with the optimal performance observed at 60 min, yielding an S/N ratio of 3.80 (Fig. 4A). Shorter incubation periods resulted in incomplete immobilitazion of the capture probe, leading to reduced hybridization efficiency and consequently lower electrochemical signals. In contrast, extending the incubation beyond 60 min did not produce a noticeable improvement in the response, indicating that surface saturation had already been reached. The concentration of the capture probe was evaluated within the range of 0.5 to 4 μM, with the best performance achieved at 2 μM (Fig. 4B). At lower concentrations, the surface coverage was insufficient, limiting the number of available hybridisation sites and resulting in reduced analytical signals, while also slightly increasing the blank response due to a higher relative contribution of non-specific interactions. Conversely, concentrations

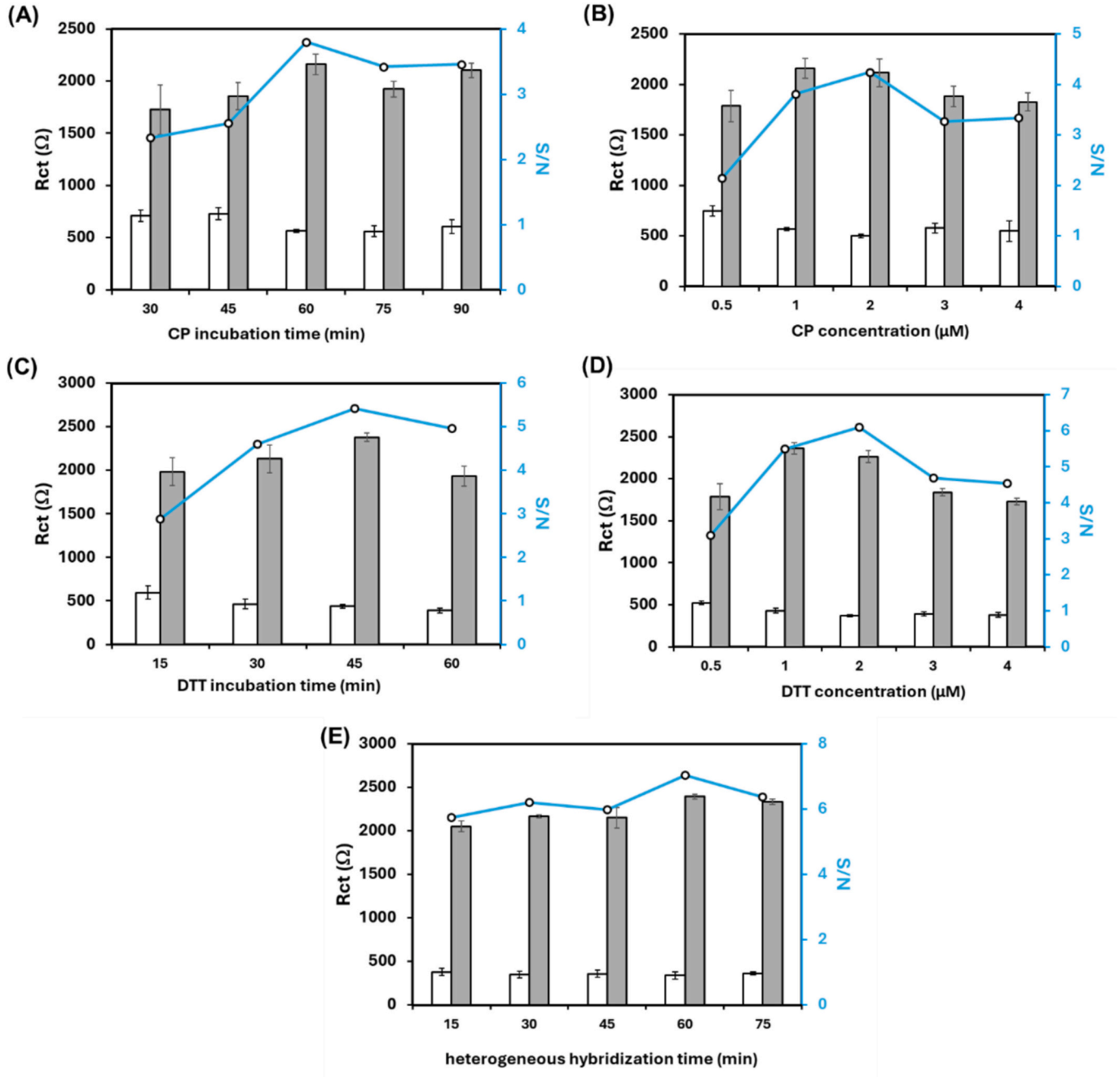

Fig. 4. Effect on the impedimetric responses measured with the biosensors in the absence (white bars) and in the presence (grey bars) of 1 nM Ara h2 DNA. CP incubation time (A), CP concentration (B), DTT incubation time (C), DTT concentration (D), and heterogeneous hybridization time (E) were evaluated. The resulting S/N values are shown as blue line. Error bars represent the standard deviation (n = 3). (For interpretation of the references to colour in this figure legend, the reader is referred to the web version of this article.)

above 2 μM did not improve the hybridization efficiency that can be attributed to steric hindrance and increased surface saturation, which reduce the accessibility of the probes for target binding. The influence of ionic strength during the immobilitazion of the capture probe on the electrode was evaluated by varying the NaCl concentration in 2× SSPE buffer from 300 to 1000 mM. The highest S/N ratio was achieved at an ionic strength of 900 mM ($S/N = 4.6$). At lower ionic strengths, stronger electrostatic repulsion between the negatively charged DNA strands led to a less organised monolayer and increased susceptibility to non-specific adsorption. In contrast, at higher ionic strengths, cations effectively screened the negative charges of the strands, promoting the formation of a denser and more ordered probe layer, which enhanced target accessibility while minimising background signals.

The optimisation of the binary SAM formation through the addition of dithiothreitol onto the CP–AuNPs–SCPE surface was also investigated, focusing on both incubation time and DTT concentration. Incubation times ranging from 15 to 60 min were studied, with the optimal response observed at 45 min (Fig. 4C). Shorter incubation times yielded incomplete monolayers with limited surface coverage, reduced probe protection, and higher blank responses from non-specific adsorption, lowering S/N. Incubation beyond 45 min may led to slight monolayer reorganisation, hindering analyte access, as reflected by the decrease in the specific signal. Similarly, DTT concentrations from 0.5 to 4 μM were evaluated, with 2 μM providing the best S/N ratio (Fig. 4D). At lower

concentrations, surface coverage was insufficient, limiting protection against non-specific adsorption and consequently increasing the background signal. Conversely, higher concentrations may facilitate the formation of a denser or multilayered film, inducing steric hindrance, with probes positioned too closely, reducing the accessibility of the target DNA and diminishing the specific signal (R_{ct} 2260 Ω for 2 μM vs R_{ct} 1729 Ω for 4 μM).

In the homogeneous hybridization process, the effects of signaling probe concentration (0.5–3 μM) and hybridization time (5–45 min) on Ara h2–SP duplex formation were evaluated. The maximum signal was achieved at 1 μM probe concentration with a hybridization period of 15 min (data not shown).Lower SP concentrations resulted in reduced hybridization efficiency due to fewer probe–target interactions, yielding weaker analytical signals, whereas higher concentrations did not further enhance the signal(i.e. S/N = 5.5 for 0.5 μM, 6.3 for 1 μM, and 5.8 for 2 μM). The optimal hybridization time was determined to be 15 min, with no significant changes in S/N observed upon longer incubation, indicating that hybridization reached equilibrium under these conditions. The influence of ionic strength during homogeneous hybridization was also assessed (300–1000 mM), showing trends similar to those observed during capture probe immobilitazion. Hybridization efficiency improved with increasing ionic strength, as electrostatic repulsion between complementary strands was mitigated, facilitating duplex formation in solution. Optimal performance was achieved at 900 mM, yielding the highest analytical signal and an S/N ratio of 6.9.

The optimisation of the heterogeneous hybridization, occurring at the electrode surface, was carried out by varying the incubation time of Ara h2-SP duplex from 15 to 75 min (Fig. 4E). The optimal response was observed at 1 h ($S/N = 7.0$). Incubation beyond 1 h did not enhance S/N, while shorter times caused incomplete hybridization, reducing analytical signals.

Table 1 summarized the variable studied and the optimal values for yielded the best analytical performance.

3.4. Analytical characteristics of the genosensor

To obtain a highly sensitive label-free DNA sensor, Ara h2 quantification study was performed using square wave voltammetry (SWV) in the presence of $[Fe(CN)_6]^{3-/4-}$ under the optimized conditions. While EIS was valuable for characterizing the electrode interface and optimizing surface modifications, in this case it did not provide sufficient sensitivity for quantitative analysis. Therefore, SWV was selected as the preferred technique for the determination of analytical parameters.

Fig. 5A displays the electrochemical responses obtained for different target concentrations, while the corresponding calibration plot is presented in Fig. 5B. Under optimized conditions, the genosensor exhibited a well-defined linear response in the concentration range of 0.025–10 nM, described by the regression equation I (μA) = (8.37 ± 0.45) C (nM) + (0.61 ± 0.05), with an excellent correlation coefficient ($R = 0.9991$). The detection (LOD) and quantification (LOQ) limits were calculated according to the conventional criterion ($\bar{x}B + 3\sigma B$ and $\bar{x}B + 10\sigma B$, $N = 10$, respectively). On this basis, the LOD was estimated at 0.02 nM and the LOQ at 0.07 nM, confirming the high sensitivity of the developed genosensor for Ara h2 DNA detection.

Table 1
Optimization of the Variables Involved in the Ara h2 DNA biosensor.

Variable	Tested range	Selected value
CP incubation time (min)	30–90	60
CP concentration (μM)	0.5–4	2
CP immobilization ionic strength (mM)	300–1000	900
DTT incubation time (min)	15–60	45
DTT concentration (μM)	0.5–4	2
SP concentration (μM)	0.5–3	1
Homogeneous hybridization time (min)	5–45	15
Homogeneous hybridization ionic strength (mM)	300–1000	900
Heterogeneous incubation time (min)	15–75	60

The precision of the biosensor was assessed at three concentration levels of Ara h2 (0.05, 1, and 10 nM), in terms of both intra-assay precision (ten measurements on the same day) and intermediary precision (eight independently fabricated DNA sensors). As shown Table 2, the RSD was in all case lower than 8 %, demonstrated the good precision of the bio-platform.

To evaluate the stability of the self-assembled monolayer (SAM), electrodes were prepared by immobilising the capture probe (1 h, 2 μM) followed by treatment with DTT (45 min, 2 μM). The electrodes were then rinsed with 2 × SSPE buffer and stored at 4 °C. The S/N ratio remained stable for up to 10 days, with decreases of approximately 15 % after 15 days and 35 % after 20 days of storage. Comparable results have been reported by other authors, Ricci et al. observed an ~50 % loss of the initial signal after three weeks in CP + MCH SAMs [39], while Dharuman et al. reported a 62 % reduction in the S/N ratio for CP + MUA + MCH SAMs after 45 days [40]. To investigate whether the observed loss of stability was related to the displacement of CP by DTT over time, or to the oxidation of the thiolated headgroup leading to its desorption from the gold surface, as other authors suggested [40], an impedimetric study was performed. The EIS analysis of SAMs after 20 days of storage revealed a markedly lower R_{ct} value compared with day one, closely resembling that of electrodes modified exclusively with DTT (Au-NPs-DTT). These results indicate that the loss of stability is primarily attributable to the release of the capture probe from the electrode surface. Por otro lado, due to the specific binding of the analyte and the fragile nature of the functionalized SAM layer, the immunosensor is single-use and cannot be reused. Due to the specificity nature of the DNA hybridization process and the inherent fragility of the self-assembled monolayer (SAM), the genosensor has been conceived as a single-use device to ensure reliable and reproducible performance.

3.5. Selectivity and analytical accuracy in real matrices

Selectivity was assessed by comparing the responses to 1 nM of the target DNA, 1 nM of a non-complementary sequence (nC), and 1 nM of a three-base mismatched sequence (nC-3) (Table S1 – Appendix). Negligible signals were observed for the nC sequence, while the nC-3 sequence produced only 16 % of the signal registered for the target, demonstrating the high selectivity of the system for specific DNA recognition of the genosensor.

The accuracy of the method, as well as its indirect assessment of matrix-related effects, was evaluated through the analysis of spiked commercial soy-based beverage and low-fat cow's milk samples. Firstly, as an additional study, a comparison between calibration curves obtained using standard solutions prepared in buffer and those prepared in soy-based beverage matrix was performed. The use of matrix-based standards showed no significant effect on the slope, considering the associated standard deviation. In the recovery study, the samples were fortified with a range of peanut Ara h2 DNA concentrations. All experiments were performed in triplicate, following the SVW protocol. As shown in Table 3, quantitative recovery values ranged from 95 % to 105.5 %, indicating that the method is both accurate and reliable, and therefore suitable for application to real samples analysis.

Enzyme-linked immunosorbent assays (ELISA), mass spectrometry, and polymerase chain reaction (PCR) are among the most widely implemented techniques for allergen detection, offering high sensitivity and specificity [11,41,42]. However, these approaches often require expensive equipment, time-consuming protocols, and specialized personnel, limiting their routine application in food control. Electrochemical biosensors have emerged as promising alternatives due to their miniaturization, cost-effectiveness, rapid response, and potential for on-site analysis [14,15]. Most reported electrochemical devices for peanut allergen detection are immunosensors or aptasensors, which rely on antibodies or aptamers as recognition elements. Immunosensors provide high affinity and selectivity, but may be costly and sensitive to protein

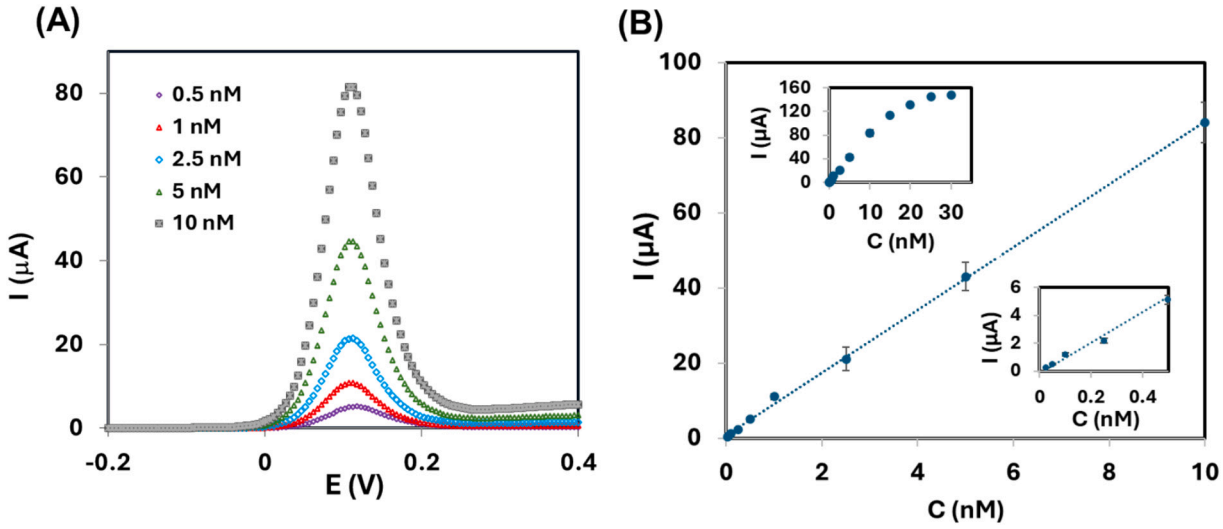

Fig. 5. (A) Square wave voltammograms recorded for different concentrations of Ara h2 under optimized experimental conditions. (B) Calibration curve showing the overall linear range; the insets display the complete calibration curve (top) and highlight the low-concentration linear region (bottom).

Table 2
Precision study of the Ara h 2 genosensor.

Concentration assayed (nM)	Intra-assay precision (RSD, %)	Intermediary precision (RSD, %)
0.05	6.5	7.2
1	5.3	6.8
10	4.5	5.3

Table 3
Recovery Studies of Ara h 2 DNA in Commercial Food Samples.

Real samples	DNA Ara h 2 add (nM)	DNA Ara h 2 found (nM)	Recovery (%)	RSD (%)
Soy-based beverage	0.1	0.095 ± 0.006	95.0	6.0
	1	1.055 ± 0.033	105.5	3.1
	10	9.870 ± 0.875	98.7	8.8
Low-fat cow's milk	0.1	0.104 ± 0.009	104.0	8.6
	1	1.045 ± 0.064	104.5	6.1
	10	9.765 ± 0.562	97.7	5.7

denaturation, while aptasensors are stable, easy to synthesize and generally less expensive [43,44]. Nevertheless, thermal or high-pressure food processing can alter protein conformation and immunoreactivity, potentially compromising protein-based assays [22]. This challenge has encouraged the development of DNA-based detection strategies. In this context, the genosensor developed in this work uses DNA as a bio-recognition element, offering high specificity through complementary hybridization, robust stability and label-free detection. These combined features simplify fabrication, reduce costs, and minimize potential interferences, making DNA-based electrochemical detection a competitive alternative for rapid and sensitive allergen analysis.

In a revision of the literature, only a limited number of DNA-based biosensors have been reported for the detection of peanut allergens. An impedimetric genosensor employing a stem-loop probe was developed for the detection of a DNA sequence specific to Ara h1. This system exploits conformational changes of the probe upon hybridization, enabling highly sensitive and selective detection, and was successfully applied to peanut-derived food samples [24]. In 2015, the same group proposed two further strategies to enhance DNA biosensor performance. One involved a multilayer graphene–gold nanocomposite on a glassy carbon electrode, providing high conductivity and large surface area, resulting in improved sensitivity and stability [26]. The other employed a chitosan–multiwalled carbon nanotube composite with a spongy gold film, increasing the effective surface area and sensitivity; additionally, enzyme amplification via biotin–streptavidin HRP enabled specific target DNA detection through electrochemical measurement of enzymatic products [25]. A voltametric electrochemical immunosensor based on gold nanoparticle-modified screen-printed carbon electrodes was developed for Ara h 6. Using a two-monoclonal antibody sandwich format and silver-based electrochemical detection, the sensor exhibited a linear range of 1–100 ng/mL, and LOD of 0.27 ng/mL [27]. The specific detection of Ara h2 is particularly important due to its high clinical relevance. Ara h2 is recognized as one of the most potent peanut allergens and is strongly associated with severe allergic reactions, including anaphylaxis, in sensitized individuals.

To our knowledge, only two DNA-based biosensors have been reported for Ara h2 detection, both relying on self-assembled monolayers (SAMs) and enzymatic amplification [26,27]. Although effective, these strategies involve additional labeling steps, which increase assay complexity, and neither has been validated in real food matrices. The first approach implemented a selective electrochemical genosensor using a sandwich format on gold electrodes with ALP-streptavidin labeling and 1-naphthyl phosphate as substrate, monitoring the enzymatically generated 1-naphthol via differential pulse voltammetry [26]. Subsequently, a ternary SAM-based sensor employed anti-fluorescein peroxidase and TMB as substrate, detecting the enzymatically oxidized TMB by chronoamperometry for indirect Ara h2 quantification [27]. This new DNA-sensor employs a label-free configuration combined with gold nanoparticles for SAM preparation, resulting in a highly sensitive and selective biosensor. Unlike previous methods [26,27], it does not require enzymatic labels, additional substrates, or complex labeling steps, which significantly reduces assay time and lowers the overall cost. Furthermore, this strategy is directly applicable to real food samples, offering a practical advantage for rapid and selective Ara h2 detection.

Although the biosensor's performance was successfully demonstrated in spiked soy-based beverages and cow's milk, the complexity and variability of real food matrices may still influence its behavior in large-scale applications. To fully validate the robustness and practical applicability of the biosensor, future studies should include a broader range of food products, particularly complex matrices with high fat or protein content, as these components can interfere with the hybridization process and the electrochemical response. Therefore, evaluating the biosensor's performance in such complex matrices is essential to ensure its reliability under real-world conditions. In this study, recovery

experiments were performed by directly adding Ara h2 DNA to the samples. However, for the quantification of naturally occurring allergen DNA in food products, a preliminary DNA extraction and purification step would be necessary prior to analysis.

4. Conclusions

This study reports the successful development of a label-free electrochemical genosensor for the detection of Ara h2, one of the major peanut allergens, employing mixed self-assembled monolayers (SAMs) for efficient DNA immobilization. Evaluation of two immobilization strategies—direct deposition of thiolated capture probe onto SPEAu and CP immobilization on AuNPs-modified SPCE—showed that gold nanoparticles enhance CP binding by increasing electrode surface area and active site density, thereby improving the sensitivity and performance of the bioplatform. A sandwich format strategy, combined with AuNPs-SPCE enabled the construction of a highly sensitive and reliable bioplatform. Among the configurations tested for sensing phase, the CP-DTT–AuNPs–SPCE system provided the best signal-to-noise ratio. The genosensor exhibited a wide dynamic range (0.025–10 nM), achieving a remarkably low limit of detection, while precision studies yielded relative standard deviations below 8 %, demonstrating robust reproducibility. Selectivity assays demonstrated negligible responses to non-complementary sequences, confirming the specificity of the system. Importantly, the method was also validated in food matrices, with satisfactory recovery values between 95 % and 105.5 %, in spiked soy-based beverages and cow's milk, supporting its applicability to food safety monitoring. However, the variability of real food matrices could affect sensor performance, so broader studies with more complex samples are needed to confirm the robustness of the platform under practical conditions. Furthermore, direct quantification of Ara h2 DNA in natural samples would require a prior DNA extraction step.

CRediT authorship contribution statement

Juan Pablo Hervás-Pérez: Writing – review & editing, Writing – original draft, Supervision, Investigation, Data curation. **Marta Sánchez-Paniagua:** Writing – review & editing, Writing – original draft, Visualization, Investigation, Formal analysis, Data curation, Conceptualization.

Declaration of competing interest

The authors declare that they have no known competing financial interests or personal relationships that could have appeared to influence the work reported in this paper.

Acknowledgements

The authors gratefully acknowledge the support of the Research Group 921114 – Plant-Based Foods: Processing, Quality and Functional Ingredients, Complutense University of Madrid (UCM), for their valuable guidance and access to resources. The funding was provided through the direct award call for Research Groups at the Complutense University of Madrid (UCM), reference GRFN24/24.

Appendix A. Supplementary data

Supplementary data to this article can be found online at https://doi.org/10.1016/j.microc.2025.116140.

Data availability

No data was used for the research described in the article.

References

[1] A. Muraro, J.W. Sublett, T. Haselkorn, C. Nilsson, T.B. Casale, Incidence of anaphylaxis and accidental peanut exposure: a systematic review, Clin. Transl. Allergy 11 (2021), https://doi.org/10.1002/clt2.12064.
[2] G.C.I. Spolidoro, M.M. Ali, Y.T. Amera, S. Nyassi, D. Lisik, A. Ioannidou, G. Rovner, E. Khaleva, C. Venter, R. van Ree, M. Worm, B. Vlieg-Boerstra, A. Sheikh, A. Muraro, G. Roberts, B.I. Nwaru, Prevalence estimates of eight big food allergies in Europe: updated systematic review and meta-analysis, Allergy 78 (2023) 2361–2417, https://doi.org/10.1111/all.15801.
[3] Regulation (EU) No 1169/2011, Regulation (EU) No 1169/2011: Document 32011R1169, 2011. http://data.europa.eu/eli/reg/2011/1169/oj (accessed September 18, 2025).
[4] S.H. Sicherer, H.A. Sampson, Food allergy: a review and update on epidemiology, pathogenesis, diagnosis, prevention, and management, J. Allergy Clin. Immunol. 141 (2018) 41–58, https://doi.org/10.1016/j.jaci.2017.11.003.
[5] R.S. Gupta, C.M. Warren, B.M. Smith, J.A. Blumenstock, J. Jiang, M.M. Davis, K. C. Nadeau, The public health impact of parent-reported childhood food allergies in the United States, Pediatrics 142 (2018), https://doi.org/10.1542/peds.2018-1235.
[6] S.J. Koppelman, S.L. Hefle, Detecting Allergens in Food, Woodhead Pub, Cambridge, 2006.
[7] O. Hemmings, G. Du Toit, S. Radulovic, G. Lack, A.F. Santos, Ara h 2 is the dominant peanut allergen despite similarities with Ara h 6, J. Allergy Clin. Immunol. 146 (2020) 621–630.e5, https://doi.org/10.1016/j.jaci.2020.03.026.
[8] N. Nicolaou, M. Poorafshar, C. Murray, A. Simpson, H. Winell, G. Kerry, A. Härlin, A. Woodcock, S. Ahlstedt, A. Custovic, Allergy or tolerance in children sensitized to peanut: prevalence and differentiation using component-resolved diagnostics, J. Allergy Clin. Immunol. 125 (2010) 191–197.e13, https://doi.org/10.1016/j.jaci.2009.10.008.
[9] A. Vereda, M. van Hage, S. Ahlstedt, M.D. Ibañez, J. Cuesta-Herranz, J. van Odijk, M. Wickman, H.A. Sampson, Peanut allergy: clinical and immunologic differences among patients from 3 different geographic regions, J. Allergy Clin. Immunol. 127 (2011) 603–607, https://doi.org/10.1016/j.jaci.2010.09.010.
[10] N.S. Alakhras, J. Shin, S.A. Smith, A.L. Sinn, W. Zhang, G. Hwang, J. Sjoerdsma, E. K. Bromley, K.E. Pollok, B. Bilgicer, M.H. Kaplan, Peanut allergen inhibition prevents anaphylaxis in a humanized mouse model, Sci. Transl. Med. 15 (2023), https://doi.org/10.1126/scitranslmed.add6373.
[11] J. Costa, T.J.R. Fernandes, C. Villa, M.B. P.P. Oliveira, I. Mafra, Advances in Food Allergen Analysis, in: Food Safety, Wiley, 2016: pp. 305–360. Doi: https://doi.org/10.1002/9781119160588.ch9.
[12] A. Sanchiz, P. Sánchez-Enciso, C. Cuadrado, R. Linacero, Detection of peanut allergen by real-time PCR: looking for a suitable detection marker as affected by processing, Foods 10 (2021) 1421, https://doi.org/10.3390/FOODS10061421/S1.
[13] A. Curulli, Recent advances in electrochemical sensing strategies for food allergen detection, Biosensors (Basel) 12 (2022) 503, https://doi.org/10.3390/bios12070503.
[14] K. Wang, X. Lin, M. Zhang, Y. Li, C. Luo, J. Wu, Review of electrochemical biosensors for food safety detection, Biosensors (Basel) 12 (2022) 959, https://doi.org/10.3390/bios12110959.
[15] K. Sheng, H. Jiang, Y. Fang, L. Wang, D. Jiang, Emerging electrochemical biosensing approaches for detection of allergen in food samples: a review, Trends Food Sci. Technol. 121 (2022) 93–104, https://doi.org/10.1016/J.TIFS.2022.01.033.
[16] Z. Xu, H. Ouyang, S. Zhao, X. Wang, X. Huo, D. He, R. Liu, Electroactive Fe3O4/α-Fe2O3@au nanocomposites driven label-free electrochemical aptasensor with magnetic self-assembly for rapid quantification of alpha-fetoprotein, Microchimica Acta 192 (2025) 1–12, https://doi.org/10.1007/S00604-025-07173-2/TABLES/3.
[17] Q. Wang, H. Ouyang, W. Li, H. Zhang, A. He, R. Liu, Development and performance evaluation of a magnetic self-assembled electrochemical biosensor based on α-Fe2O3/Fe3O4 heterogeneous nanorods for supersensitive detection of KRAS, Colloids Surf. A Physicochem. Eng. Asp. 715 (2025) 136624, https://doi.org/10.1016/J.COLSURFA.2025.136624.
[18] Q. Wang, M. Liu, J. Zhao, J. Yuan, S. Li, R. Liu, Development of a magnetic α-Fe2O3/Fe3O4 heterogeneous nanorod-based electrochemical biosensing platform for HPV16 E7 oncoprotein detection, Int. J. Biol. Macromol. 284 (2025), https://doi.org/10.1016/J.IJBIOMAC.2024.138085.
[19] M. Freitas, M.M.P.S. Neves, H.P.A. Nouws, C. Delerue-Matos, Electrochemical Immunosensor for the simultaneous determination of two Main Peanut allergenic proteins (Ara h 1 and Ara h 6) in food matrices, Foods 10 (2021) 1718, https://doi.org/10.3390/foods10081718.
[20] H. Jiang, Q. Guo, C. Zhang, Z. Sun, X. Weng, Microfluidic origami nano-aptasensor for peanut allergen Ara h1 detection, Food Chem. 365 (2021) 130511, https://doi.org/10.1016/j.foodchem.2021.130511.
[21] Y. Hu, J. Lin, L. Peng, Y. Wang, S. Wu, X. Ji, H. Lv, J. Wu, Y. Zhang, S. Wang, Nanobody-based electrochemical immunoassay for sensitive detection of Peanut allergen Ara h 1, J. Agric. Food Chem. 71 (2023) 7535–7545, https://doi.org/10.1021/acs.jafc.3c00921.
[22] K.C.M. Verhoeckx, Y.M. Vissers, J.L. Baumert, R. Faludi, M. Feys, S. Flanagan, C. Herouet-Guicheney, T. Holzhauser, R. Shimojo, N. van der Bolt, H. Wichers, I. Kimber, Food processing and allergenicity, Food Chem. Toxicol. 80 (2015) 223–240, https://doi.org/10.1016/j.fct.2015.03.005.
[23] B. Martín-Fernández, C.L. Manzanares-Palenzuela, M. Sánchez-Paniagua López, N. de-los-Santos-Álvarez, B. López-Ruiz, Electrochemical genosensors in food safety assessment, Crit. Rev. Food Sci. Nutr. 57 (2017) 2758–2774. Doi: https://doi.org/10.1080/10408398.2015.1067597.

[24] X. Sun, L. Guan, X. Shan, Y. Zhang, Z. Li, Electrochemical Detection of Peanut Allergen Ara h 1 Using a Sensitive DNA Biosensor Based on Stem–Loop Probe, J. Agric. Food Chem. 60 (2012) 10979–10984, https://doi.org/10.1021/jf3027233.
[25] X. Sun, M. Jia, L. Guan, J. Ji, Y. Zhang, L. Tang, Z. Li, Multilayer graphene–gold nanocomposite modified stem-loop DNA biosensor for peanut allergen-Ara h1 detection, Food Chem. 172 (2015) 335–342, https://doi.org/10.1016/j.foodchem.2014.09.042.
[26] X. Sun, M. Jia, J. Ji, L. Guan, Y. Zhang, L. Tang, Z. Li, Enzymatic amplification detection of peanut allergen Ara h1 using a stem-loop DNA biosensor modified with a chitosan-mutiwalled carbon nanotube nanocomposite and spongy gold film, Talanta 131 (2015) 521–527, https://doi.org/10.1016/j.talanta.2014.07.078.
[27] R.C. Alves, F.B. Pimentel, H.P.A. Nouws, W. Correr, M.B. González-García, M.B.P. P. Oliveira, C. Delerue-Matos, Detection of the peanut allergen Ara h 6 in foodstuffs using a voltammetric biosensing approach, Anal. Bioanal. Chem. 407 (2015) 7157–7163, https://doi.org/10.1007/S00216-015-8879-8/FIGURES/4.
[28] M. Gamella, M.I. Ballesteros, V. Ruiz-Valdepeñas Montiel, A. Sánchiz, C. Cuadrado, J.M. Pingarrón, R. Linacero, S. Campuzano, Disposable amperometric biotool for peanut detection in processed foods by targeting a chloroplast DNA marker, Talanta 277 (2024) 126350, https://doi.org/10.1016/j.talanta.2024.126350.
[29] M.S.-P. López, G.F. Cabanillas, M.J.L. Castañón, B. López-Ruiz, Development of a genosensor for peanut allergen ARA h 2 detection and its optimization by surface response methodology, Biosens. Bioelectron. 62 (2014) 350–356, https://doi.org/10.1016/j.bios.2014.06.065.
[30] J. Aufartova, M.S. López, B. Martín-Fernández, B. López-Ruiz, Key factors of ternary monolayers to improve DNA sensors performance, Electroanalysis 29 (2017) 131–139, https://doi.org/10.1002/elan.201600538.
[31] P.A. Rasheed, N. Sandhyarani, Electrochemical DNA sensors based on the use of gold nanoparticles: a review on recent developments, Microchimica Acta 184 (2017) 981–1000, https://doi.org/10.1007/s00604-017-2143-1.
[32] A. Karnwal, R.S. Kumar Sachan, I. Devgon, J. Devgon, G. Pant, M. Panchpuri, A. Ahmad, M.B. Alshammari, K. Hossain, G. Kumar, Gold nanoparticles in Nanobiotechnology: from synthesis to biosensing applications, ACS, Omega 9 (2024) 29966–29982, https://doi.org/10.1021/acsomega.3c10352.
[33] T. Jamshidnejad-Tosaramandani, S. Kashanian, K. Omidfar, H.B. Schiöth, Recent advances in gold nanostructure-based biosensors in detecting diabetes biomarkers, Front. Bioeng. Biotechnol. 12 (2024), https://doi.org/10.3389/fbioe.2024.1446355.
[34] M. Sharma, P. Mahajan, A.S. Alsubaie, V. Khanna, S. Chahal, A. Thakur, A. Yadav, A. Arya, A. Singh, G. Singh, Next-generation nanomaterials-based biosensors: real-time biosensing devices for detecting emerging environmental pollutants, Mater Today Sustain 29 (2025) 101068, https://doi.org/10.1016/j.mtsust.2024.101068.
[35] L. Yin Zhou, X. Yuan Zhang, G. Lin Wang, X. Xia Jiao, H. Qun Luo, N. Bing Li, A Simple and Label-Free Electrochemical Biosensor for DNA Detection Based on the Super-Sandwich Assay †, (n.d.). Doi: https://doi.org/10.1039/c2an35905g.
[36] Y. Zhang, C. Pilapong, Y. Guo, Z. Ling, O. Cespedes, P. Quirke, D. Zhou, Sensitive, simultaneous quantitation of two unlabeled DNA targets using a magnetic nanoparticle−enzyme Sandwich assay terms of use CC-BY, Anal. Chem. 85 (2013) 9244, https://doi.org/10.1021/ac402081u.
[37] S. Campuzano, F. Kuralay, J. Wang, Ternary Monolayer Interfaces for Ultrasensitive and Direct Bioelectronic Detection of Nucleic Acids in Complex Matrices, (n.d.). Doi: https://doi.org/10.1002/elan.201100452.
[38] M. Sánchez-Paniagua, S. Palenzuela-Batista, C.L. Manzanares-Palenzuela, B. López-Ruiz, Electrochemical genosensor for Klotho detection based on aliphatic and aromatic thiols self-assembled monolayers, (2020). Doi: https://doi.org/10.1016/j.talanta.2020.120735.
[39] F. Ricci, N. Zari, F. Caprio, S. Recine, A. Amine, D. Moscone, G. Palleschi, K.W. Plaxco, Surface chemistry effects on the performance of an electrochemical DNA sensor, (2009). Doi: https://doi.org/10.1016/j.bioelechem.2009.03.007.
[40] V. Dharuman, K. Vijayaraj, S. Radhakrishnan, T. Dinakaran, J.S. Narayanan, M. Bhuvana, J. Wilson, Sensitive label-free electrochemical DNA hybridization detection in the presence of 11-mercaptoundecanoic acid on the thiolated single strand DNA and mercaptohexanol binary mixed monolayer surface, Electrochim. Acta 56 (2011) 8147–8155, https://doi.org/10.1016/j.electacta.2011.05.115.
[41] Y. Shencheng, M. Zhou, Y. Zhao, S. Li, H. Lin, M.F. Abdallah, R. Zhang, S. Liu, Y. Li, S. Yang, Development and validation of a QconCAT-based LC-MS/MS method for the quantification of 12 food allergens in foods, J. Agric. Food Chem. 73 (2025) 18974–18986, https://doi.org/10.1021/ACS.JAFC.5C03044/ASSET/IMAGES/LARGE/JF5C03044_0003.JPEG.
[42] A.C. Eischeid, Droplet digital PCR for detection of allergenic peanut in food ingredients, JSFA Reports 5 (2025) 362–369, https://doi.org/10.1002/JSF2.70013.
[43] R. Khodaei, A. Ahmady, S.M. Khoshfetrat, S. Kashanian, S.M. Tavangar, K. Omidfar, Voltammetric immunosensor for E-cadherin promoter DNA methylation using a Fe 3 O 4 -citric acid nanocomposite and a screen-printed carbon electrode modified with poly(vinyl alcohol) and reduced graphene oxide, Microchim. Acta 186 (2019) 1–12, https://doi.org/10.1007/S00604-019-3234-Y/TABLES/4.
[44] M. Sadeghi, S. Kashanian, S.M. Naghib, E. Askari, F. Haghiralsadat, D. Tofighi, A highly sensitive nanobiosensor based on aptamer-conjugated graphene-decorated rhodium nanoparticles for detection of HER2-positive circulating tumor cells, Nanotechnol. Rev. 11 (2022) 793–810, https://doi.org/10.1515/NTREV-2022-0047/ASSET/GRAPHIC/J_NTREV-2022-0047_FIG_008.JPG.